Stable, single-layer structure of Group V elements.

Fatih Ersan,[1] Ethem Aktürk,[1,2,3,*] and Salim Ciraci[3,†]

[1] *Department of Physics, Adnan Menderes University, 09100,Aydın, Turkey*
[2] *Nanotechnology Application and Research Center, Adnan Menderes University, Aydın 09010, Turkey*
[3] *Department of Physics, Bilkent University, 06800 Ankara, Turkey*

In addition to stable, single-layer buckled honeycomb and washboard structures of group V elements (or pnictogens P, As, Sb, Bi) we showed that these elements can form also two dimensional, single-layer structures consisting of buckled square and octagon rings. An extensive analysis comprising calculation of mechanical properties, vibration frequencies and finite temperature ab-initio molecular dynamics confirm that these structures are dynamically and thermally stable and suitable for applications at room temperature and above it. All these structures are semiconductors with fundamental band gap, which is wide for P, but decreases with increasing row number. The effect of the spin-orbit coupling decreases the band gap and is found to be crucial for Sb and Bi. These results are obtained from first-principles calculations based on density functional theory.

I. INTRODUCTION

The element(s) and its atomic structure are crucial for the physical and chemical properties of 2D materials. Hopes in finding the contender of graphene[1,2] have initiated searches for new 2D materials of other elements in diverse structures. The synthesis of single-layer of hexagonal h-BN[3] and h-MoS_2,[4] have been achieved quickly, since their parent layered crystals have weak interlayer interactions like graphite. In the mean time, the stability of similar single-layer (SL) hexagonal (h), as well as (T) structures of several transition metal oxides and dichalcogenides have been predicted[5] showing diversity of electronic and magnetic properties. On the other side, the tremendous experience accumulated through silicon technology rendered the synthesis of SL hexagonal Si a prioritized research field even if this element has no 3D layered allotrope like graphite. Interestingly, theoretical studies[6,7] have shown that Si, as well as Ge can, in fact, form stable, SL honeycomb structures with hexagonal lattices, if alternating atoms at the corners are buckled to assure the stability in 2D. Later, silicene and germanene have been synthesized on Ag and Au substrates.[8,9] Theoretical studies went further to include compounds of Group IV elements, as well as compounds III-V and II-VI elements in the study of stability; majority of them were demonstrated to form stable SL honeycomb structures.[10–13] Other manifolds zinc blende compounds, such as tetragonal and V-shaped, were also predicted.[14] Much recently, AlN and GaN in honeycomb structures have been also synthesized.[15,16]

Apart from the honeycomb structures of graphene, other allotropes, like graphynes and graphdiynes were also considered.[17–21] Theoretical studies predicted that α, β, and γ graphynes are stable; while α and β graphynes preserve Dirac cones, γ graphyne is a semiconductor due to Kekule distortion effect[22,23]. Sharma *et al.*[24] predicted sp^2 hybridized 2D allotrope of carbon, named as pentahexoctite having mechanical strength comparable to graphene. In addition, Zhang *et al.*[25] predicted five atomically thin, free-standing germanium selenide (GeSe) polymorps, which have high kinetic stability and energy band gaps in the visible region. It has been shown that MoS_2, which is normally a semiconductor in SL honeycomb structure, possesses both massless Dirac and heavy fermions when it is formed in planar, SL square/octagon-, or *s/o*-structure with 2D square lattice.[26].

After the synthesis of very thin films of phosporus[27] researchers start to seek similar structures in other group V elements or pnictogens. Recent theoretical studies have predicted that nitrogen,[28] phosphorus,[29–31] arsenic,[32–35] antimony,[36–39] bismuth[40–43] and compounds of group V-V elements[44] can form stable, freestanding SL, planar as well as buckled honeycomb (*b*-) structures similar to that of silicene and germanene, and also other manifolds, such as SL symmetric (*w*-)and asymmetric washboard (*aw*-) structures and others. These SL phases are named, respectively as *nitrogene, phosphorene, arsenene, antimonene* and *bismuthene*. It should be noted that phosphorus, arsenic, antimony and bismuth have stable, 3D quasi layered parent crystals, which corroborate efforts to synthesize SL or very thin films (or multilayers) of these elements. Among the possible non-honeycomb structures of phosphorus, Guan *et al.*[30] and Wu *et al.*,[31] proposed a *s/o*-type structure consisting of square and octagon rings. However, neither dynamical, thermal and other stability analysis of these structures was performed to show that whether they are really stable, nor any relevant structural parameters, such as buckling distance, short and long bonds, bond angles, pertinent mechanical properties and critical energetics etc. were provided to characterize the *s/o*-structure. Recently, Kou *et al.*[45] pointed out that buckled *s/o*-structure (they named as tetragonal bilayer) of Bi is stable and exhibits topological insulator features.

Earlier, we have studied SL pnictogen phases consisting of planar and buckled honeycomb, symmetric and asymmetric washboard structures, whereby their dynamical and thermal stability, mechanical, electronic, magnetic and optical properties were revealed and also

their functionalization with selected single atoms and molecules were investigated.[21,34–36,43] In those studies crucial effects of the structures on physical properties were revealed. In this paper, we present a systematic study of pnictogens in SL freestanding, buckled s/o-structures. Since our tests resulted in an instability of SL nitrogene in s/o-structure, our study comprises only P, As, Sb and Bi among group V elements. Having assured that they are dynamically and thermally stable, we calculated their mechanical and electronic properties using density functional theory (DFT) and compared them with the properties of other SL phases of pnictogens. These structures are semiconductors with wide to narrow band gap, depending on the type of constituent group V elements. The effect of the spin-orbit coupling becomes crucial for s/o-Sb and s/o-Bi; but band energies calculated within DFT require correction. Interesting correlations of the physical properties of s/o-structures among pnictogens are also revealed.

II. METHOD

Our theoretical analysis and predictions are obtained from first-principles pseudopotential calculations based on both the spin-polarized and spin-unpolarized density functional theory within the generalized gradient approximation (GGA) including van der Waals corrections[46]. Here we used projector-augmented wave (PAW) potentials[47] and the exchange-correlation potential is approximated with Perdew-Burke-Ernzerhof (PBE) functional[48]. Numerical calculations were carried out using the VASP software.[49]. A plane-wave basis set with kinetic energy cutoff is taken to be $\hbar^2|\mathbf{k}+\mathbf{G}|^2/2m =$ 400 eV. The Brillouin zones (BZ) were sampled in the $\mathbf{k}$-space within Monkhorst-Pack[50] scheme by (16 $\times$ 16 $\times$ 1) mesh. Atomic positions were optimized using the conjugate gradient method, where the total energy and atomic forces were minimized. The energy convergence value between two consecutive steps was chosen as 10^{-5} eV. A maximum force of 0.002 eV/Å was allowed on each atom. Gaussian type Fermi-level smearing method is used with a smearing width of 0.01 eV. In the periodically repeating slab model, the vacuum spacing between the layers are set to 15 Å to minimize the interlayer coupling. Phonon dispersion curves are obtained by using the finite displacement method (for 2×2 supercells) as implemented in the PHONOPY[51] code without spin-orbit coupling (SOC). Additionally, the thermal stability analysis of the optimized structures was tested by using finite temperature *ab-initio* molecular dynamics (MD) calculations. A Nosé thermostat is used and Newton's equation of motion is integrated through the Verlet algorithm with time steps of 2fs.

Self-consistent field calculations of the electronic energy bands, total and orbital projected densities of states corresponding to the optimized structure were carried out with and without spin-orbit coupling (SOC). Since the fundamental band gaps are underestimated by standard DFT, we applied correction to PBE results using the screened hybrid functional, HSE06 method[52–55]. The screening length of HSE06 is taken as λ=0.2 Å^{-1}, and the mixing rate of the HF exchange potential is set to 0.25.

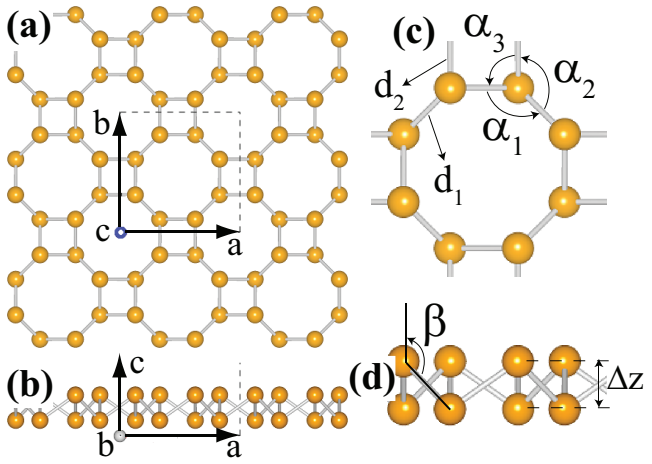

Figure 1. Description of the atomic configuration and structural parameters of buckled s/o-structure. a) Top view of the atomic structure consisting of square and octagon rings. The square unit cell with lattice constants **a**=**b** is delineated with dashed lines. b) Side view consisting of two parallel atomic planes as a result of buckling. c) An octagon ring of the s/o-structure with relevant bonds d_1, d_2 and bond angles α_1, α_2, α_3. d) Side view of the octagon showing the buckling parameter, Δz and bond angle β.

III. STRUCTURE AND ENERGETICS

In Fig. 1 SL buckled s/o-structure together with the major structural parameters and rectangular unit cell is shown. Even if the xy-projection of the structure appears to be formed from square and octagon rings, it actually consists of buckled square and octagon rings. The stability of the structure is maintained by the buckling of planar structure, whereby atoms at alternating corners are buckled by Δz. This way, a SL structure consists of two atomic planes. All corners of the rings are occupied by the same atoms of Group V elements, namely P, As, Sb and Bi. The unit cell comprises 8 atoms at the corners of an octagon, which are connected by bonds, four of them, d_1, are shared by four adjacent octagons. The remaining four, d_2 are shared by square rings. This way one distinguishes two different bonds, d_1 and d_2, where d_1 is slightly shorter than d_2. The percentage difference, $d_2 - d_1/d_1$ increases from 0.9% to 3% as one goes from P to Bi. The average of d_1 and d_2 of s/o-X approximately equals to the bond length, d of b-X. The s/o-X is an open structure relative to b-X with the ratio of the areal atom density, 0.8 for P. This ratio decreases with increasing

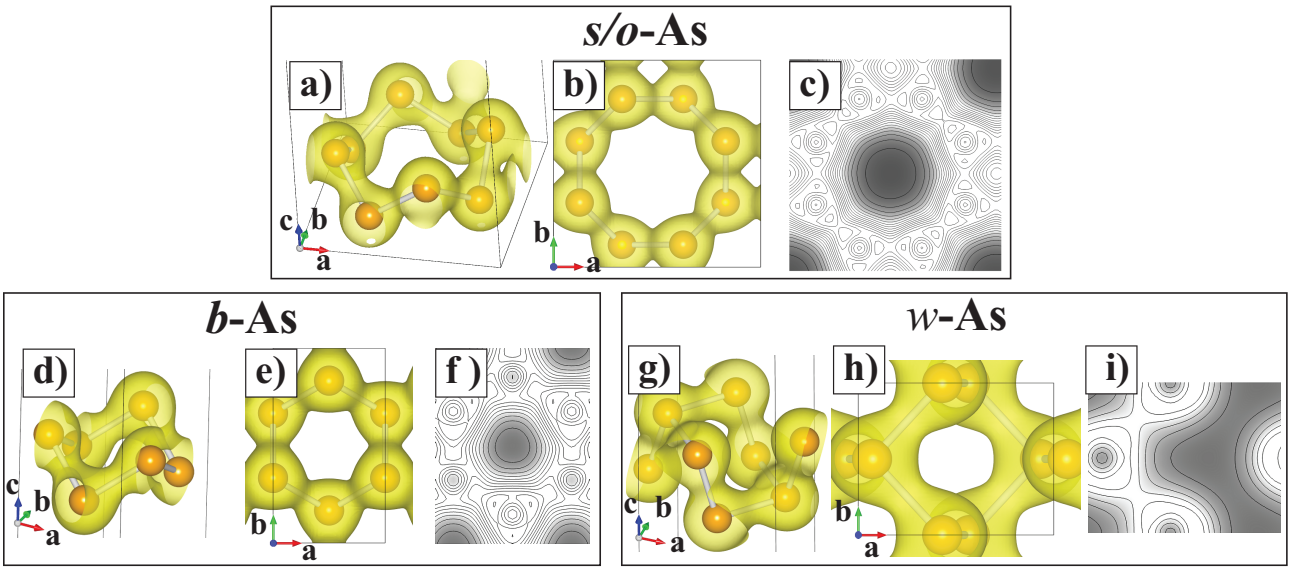

Figure 2. Total charge density plots of buckled s/o-As, b-As and w-As. a) Tilted view; b) Top view of the charge density isosurfaces on an octagon ring. c) Contour plots of the total charge density on a plane passing through xy-plane (parallel to atomic planes), which bisects Δz. d-f) Same for b-As and g-i) for w-As. Isosurface and contour spacing values are 0.05 electrons/Å^3 and 0.015 electrons/Å^3, respectively.

row number of X and becomes 0.75 for Bi. Similar analysis can be carried out also using areal packing fraction. All atoms are threefold coordinated in s/o-X structure; the bonds connecting any atom to its three nearest neighbors are not coplanar. Consequently, the hybridization of bonds deviates from sp^2 and acquires also p_z orbital contribution.

Structural parameters, as well as, lattice constants presented in Fig. 1 are optimized. The energetics, elastic constants, phonon frequencies and electronic structures are calculated in terms of these optimized lattice constants. In Table I the values of structural parameters, elastic constants calculated for s/o-X structures are compared with those of b-X, w-X and aw-X (X=P, As, Sb and Bi) structures. Notably, the lattice constants $a = b$, bond lengths $d_{1,2}$, and the buckling Δz, increase with increasing row number of X-atom. The average bond length of s/o-X, b-X and w-X structures are approximately equal, but s/o-X and b-X have relatively smaller buckling parameter. In the rest of the text, the identification, SL buckled, in front of s/o will be dropped for the sake of brevity.

In Fig. 2 the isosurfaces of the total charge density of s/o-As, b-As and w-As are shown. Because of differences in the hybridization of hybrid orbitals in different bonds in s/o-As, the overall charge density distribution of these structure appear to be different.

As for the energetics of these structures, the cohesive energy and the formation energy at T=0 is relevant. The cohesive energy per atom of s/o-X structures, $E_c = E_T[X] - E_T[s/o - X]/8$ is obtained from the difference between the total energy of a free X-atom and that of the corresponding s/o-X per atom. By definition $E_c > 0$ indicates binding. The formation energy E_f at $T = 0$ is obtained by subtracting the cohesive energy of 3D bulk crystal of X element from the cohesive energy of the s/o-X structure. In Table II, the energetics of 3D bulk, s/o-X, b-X, w-X and aw-X are compared. The cohesive energy of s/o-X structure is consistently 0.16 eV - 0.27 eV per atom smaller than the most energetic SL structure of X elements. However, this small difference does not imply that s/o-X structures cannot be synthesized and/or they cannot remain stable at room temperature. All these structures have positive binding energy, but have negative formation energy. Accordingly, the optimized s/o-X phases may correspond to local minima on the Born-Oppenheimer surfaces as other structures. This situation necessitates an extensive stability analysis of each s/o-X structures in the next section.

IV. STABILITY ANALYSIS

Our analysis of stability starts with the calculation of the mechanical properties of the s/o-X optimized structures. To this end we calculate the in-plane stiffness,[56] $C_{x,y} = (1/A)\partial E_T^2/\partial \epsilon_{x,y}^2$ and Poisson's ratio $\nu_{xy} = \epsilon_y/\epsilon_x$. In these expressions, A is the area of the unit cell, E_T is the total energy per cell of the s/o-X structure, and ϵ_x is the uniaxial strain along x-axis. We note that $C_x = C_y$ and $\nu_{xy} = \nu_{yx}$. Calculated values listed in Table I indicate that the in-plane stiffness of s/o-X structure is smaller than that of b-X, w-X and aw-X structures. This is mainly due to the fact that s/o-X is more open than other structures. Nevertheless, all s/o-X phases have positive in-plane stiffness, which decreases with increasing

Table I. Comparison of the calculated values of s/o-X structures with those of b-X, w-X and aw-X (X=P, As, Sb, and Bi) structures. Values without references are calculated in the present study. Square lattice constants, $a = b$; bond lengths, d_i (i=1,2); selected bond angles, α_i (i=1,2,3), β; buckling parameter, Δz; in-plane stiffness $C_x = C_y$; Poisson's ratio ν_{xy}=ν_{yx}.

	Structure	Lattice (Å)	d_i (Å)	α_i, β (i=1,2,3; degree)	Δz (Å)	C_x=C_y (J/m^2)	ν_{xy}=ν_{yx}
P	s/o	a=b=6.54	d_1=2.26, d_2=2.28	α_1=100.6 ; α_2=100.7	1.25	$C_{x,y}$=32.06	ν_{xy}=0.532
				α_3=72.4 ; β=123.7			
	b	a=b=3.28, 3.28[57]	2.27, 2.26[57]	92.9, 92.9[57]	1.24, 1.24[57]	$C_{x,y}$=75.45	ν_{xy}=0.107
	w	a=3.31, 3.30[58,59]	d_1=2.22, 2.22[58,59]	96[58,59],104[58,59]	2.51[59]	C_x=44[59],41.3[60]	ν_{xy}=0.17[59]
		b=4.55, 4.62[58,59]	d_2=2.25, 2.26[58,59]	96.1 , 103.5	2.12	C_y=166[59], 106.4[60]	ν_{yx}=0.62[59]
As	s/o	a=b=7.06	d_1=2.48, d_2=2.52	α_1=99.1 ; α_2=99.4	1.42	$C_{x,y}$=20.87	ν_{xy}=0.599
				α_3=71.8 ; β=124.7			
	b	a=b=3.60, 3.61[32]	2.50, 2.50[32]	91.9, 92.2[32]	1.40	$C_{x,y}$=51.41	ν_{xy}=0.165
	w	a=3.67, 3.68[32]	d_1=2.50, 2.50[32]	94.6[32], 100.8[32]		C_x= 29[33]	
		b=4.72, 4.77[32]	d_2=2.47, 2.49[32]	94.7, 100.6	2.38	C_y=74.7[33]	
Sb	s/o	a=b=8.01	d_1=2.85, d_2=2.91	α_1=97.4 ; α_2=97.5	1.67	$C_{x,y}$=11.55	ν_{xy}=0.663
				α_3=70.6 ; β=126.1			
	b	a=b=4.04, 4.12[61]	2.87, 2.89[61]	89.6, 89[36]	1.67, 1.65[61]	$C_{x,y}$=34.56	ν_{xy}=0.192
	aw	a=4.78, 4.74[39]	d_1=2.85, 2.87[39]	95.3[39], 102.4[39]		C_x= 12[36]	ν_{xy}=0.36[36]
		b=4.27, 4.36[39]	d_2=2.91, 2.94[39]	94.4, 103.5	0.38, 2.82	C_y= 29[36]	ν_{yx}=1.20[36]
Bi	s/o	a=b=8.40	d_1=2.99, d_2=3.08	α_1=96.6 ; α_2=96.7	1.78	$C_{x,y}$=7.61	ν_{xy}=0.728
				α_3=70.4 ; β=126.7			
	b	a=b=4.19, 4.33[61]	3.01, 3.09[61]	87.11	1.80, 1.71[61]	$C_{x,y}$=29.61	ν_{xy}=0.232
	aw	a=4.87, 4.94[43]	d_1=3.08, 3.11[43]	92.0, 107.4	0.5[43]	C_x=10.03[43]	ν_{xy}=0.261[43]
		b=4.44, 4.55[43]	d_2=3.03, 3.10[43]	92.2, 106.7	0.57, 2.72	C_y=25.5[43]	ν_{yx}=0.648[43]

Table II. Comparison of the calculated cohesive energies ,E_c, of s/o-X structures with the cohesive energies of 3D bulk crystals, b-X, w-X and aw-X (X=P, As, Sb, and Bi) structures. Formation energies at T=0 K, E_f, are given in square brackets.

	Bulk (eV/atom)	b-X (eV/atom)	w-X (eV/atom)	aw-X (eV/atom)	s/o-X (eV/atom)
P	3.67	3.55 [-0.12]	3.59 [-0.08]	-	3.43 [-0.24]
	3.33[62]	3.47[63]	3.48[58]		
	3.49-4.74[64]	3.42[65]			
	3.43[66]	3.29[66]	3.30[66]		
	3.79[67]				
As	3.30	3.14 [-0.16]	3.13 [-0.17]	-	2.98 [-0.32]
	2.99[32]	2.99[32]	2.95[32]		
		3.15[68]	3.13[68]		
		2.95[69]			
		2.96[70]			
Sb	3.13	2.86 [-0.27]	-	2.89 [-0.24]	2.69 [-0.44]
	2.75[71,72]	4.26[39]	-	4.29[39]	
	3.12[36]	2.87[36]	2.88[36]	2.89[36]	
Bi	3.12	2.77 [-0.36]	-	2.84 [-0.28]	2.57 [-0.56]
	3.22[41]	1.95[43]	1.97[43]	1.97[43]	
		1.97[40]			
		4.45[45]			4.25[45]

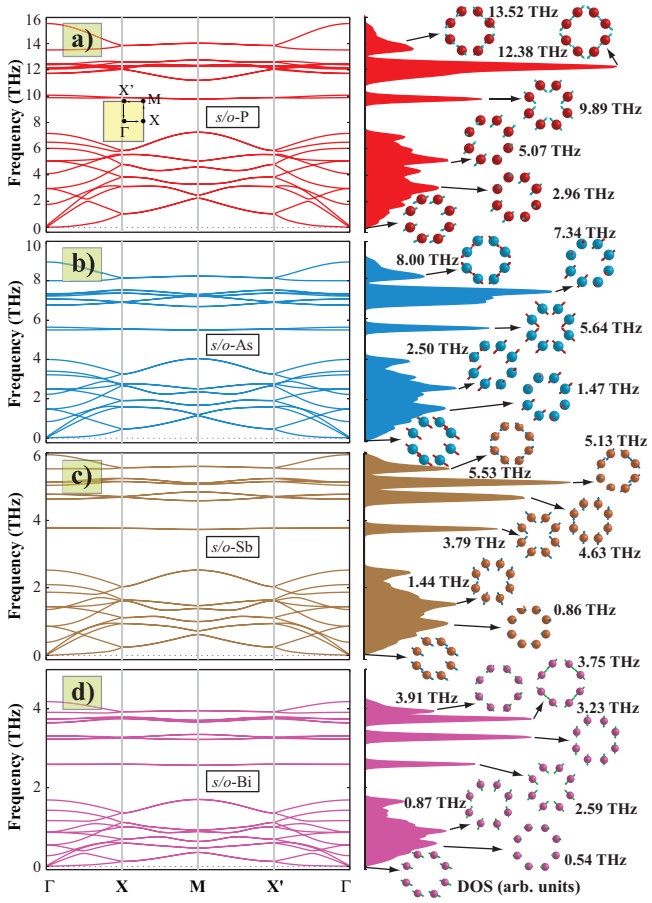

Figure 3. a)-d) Phonon bands i.e. frequency f versus $\mathbf{k}$ along the selected symmetry axis of the square Brillouin zone shown by inset and corresponding total densities of states. Special modes corresponding to selected singularities are shown by insets.

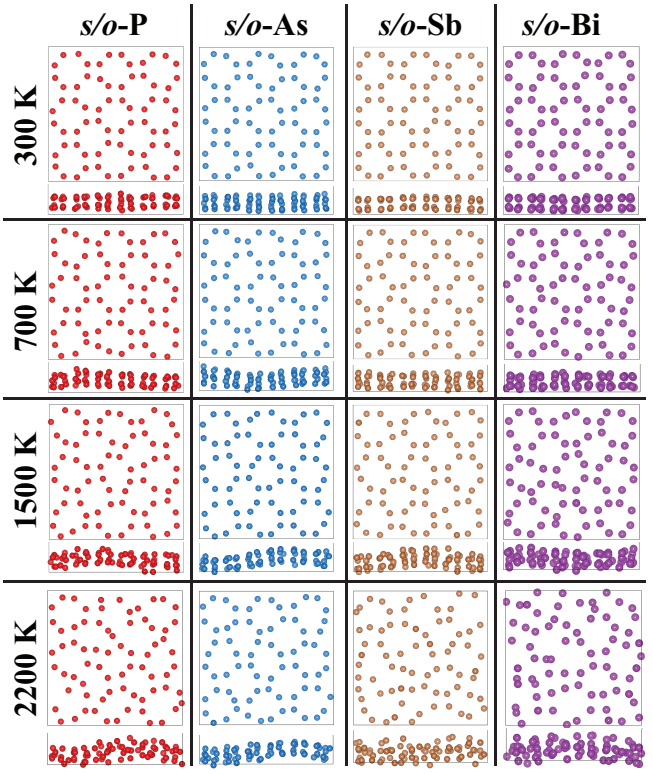

Figure 4. Top and side views of the snapshots of the atomic configurations of s/o-X (X=P, As, Sb and Bi) structures taken from MD simulations carried out at different temperatures.

row number of X. Note that the difference between in-plane stiffness of b-X and s/o-X increases with the row number of X complies with the fact that the areal atom density decreases with increasing row number.

We will deduce from the present analysis whether s/o-X structures correspond to local minima in the Born-Oppenheimer surface and whether these minima are deep enough to provide stability against thermal excitations. Stability tests in the present study cover dynamical stability at T=0K and high-temperature thermal stability. In the former, the vibration frequencies $f(\mathbf{k}) = \Omega(\mathbf{k})/2\pi$ of a given s/o-X structure in the $\mathbf{k}$-space are calculated. The structure is considered dynamically stable at T=0 K, only if all vibration frequencies in BZ $f(\mathbf{k}) > 0$. The calculated vibration frequencies of all s/o-X (X=P, As, Sb and Bi) structures are found to be positive and hence confirm the dynamical stability of these four structures at T=0. In Fig. 3, we present the dispersions of the vibration frequencies $f = (\mathbf{k})$ along symmetry directions (or phonon bands) and the densities of states. The modes corresponding to specific frequencies are also described.

The overall distributions of the vibration frequencies are similar in s/o-X structures, except that their widths and frequencies of singular points in densities of states raise with decreasing row numbers of elements. It should be noted that for elements having low row numbers, the X-X bonds are relatively shorter and conversely force constants are relatively stronger leading to relatively higher vibration frequencies.

The thermal stability at high temperature, which is crucial from the technological application point of view of s/o-X structures, indicates that local minimum of a s/o-X structure is deep. This is tested by *ab-initio* molecular dynamics (MD) calculations. Here any s/o-X structure preserving its overall shape at high temperature for the time scale of picoseconds and keeping its optimized atomic configuration as $T \to 0$ can assure that it is stable at room temperature and perhaps slightly above. In Fig. 4 we show the snapshots of atomic configurations of s/o-X structures taken from MD simulations at various temperature. In the course of MD iterations lasting 2 picoseconds at 1500 K the identity of the s/o-structure is remained, especially for P and As. Severe and irreversible distortions start to occur from 1500 K on for heavier elements for Sb and Bi.

Based on calculated values of mechanical properties, dynamical, as well as thermal stability tests, which were performed in picosecond time scale at temperatures as

high as 2200 K, one concludes that four free standing s/o-X structures considered in this paper can be stable at room temperature and at least slightly above it. This conclusion renders the electronic properties of these four s/o-structures worthy of investigation for possible applications.

V. ELECTRONIC PROPERTIES

Understanding the physical properties, in particular electronic energy bands of stable s/o-X structures is the prime motivation of the present study. The electronic structure of the optimized and stable s/o-X (X=P, As, Sb and Bi) structures will be investigated in this section. The electronic band structures calculated along the selected directions of BZ within PBE, PBE+SOC, HSE and HSE+SOC are presented in Fig. 5. Comparing these bands, the effects of spin-orbit coupling, as well as HSE correction over DFT values are revealed. In addition, results of recent calculations on the energy bands of different structures, such as b-X, w-X and aW-X (X=P, As, Sb and Bi), will be compared in order to better understand the present s/o-structure. Values of the fundamental band gaps calculated with PBE method together with the band gaps of b-X, w-X and aw-X structures calculated earlier are listed in Table. III.

The fundamental band gap calculated using PBE is indirect and is 2.16 eV for s/o-P, but becomes direct for s/o-structures of heavier group V elements and decreases with increasing row numbers. s/o-Bi has smallest PBE band gap, $E_{g,d}$ =0.63 eV. The effect of SOC is negligible for s/o-P, but becomes significant starting from s/o-As and increases with increasing row number of group V elements. Upon inclusion of SOC to PBE calculations, the fundamental band gaps decrease by 0.11 eV, 0.29 eV and 0.29 eV in s/o-As, s/o-Sb and s/o-Bi, respectively. Moreover, through the Rashba-type splitting, the fundamental band gap of s/o-Bi changes from direct to indirect and becomes $E_{g,i}$ =0.34 eV. The present values of the fundamental band gap of s/o-Bi is in good agreement with those reported by Kou et al.[45]

Since the fundamental band gaps are normally underestimated by DFT, the band structures are also calculated using the HSE correction. After HSE correction to PBE bands, the fundamental band gaps of s/o-X structures generally increase, but the direct/indirect character of the fundamental band gaps are unaltered. The effect of HSE correction is large for s/o-P and is 0.76 eV, but decreases with increasing row number of X. Namely, the correction is 0.68 eV, 0.53 eV, and 0.38 eV, for s/o-As, s/o-Sb, and s/o-Bi, respectively. After the inclusion of SOC to HSE correction, the band gap of s/o-P becomes unaltered and remains to be indirect. However, even if its character unchanged upon the inclusion of SOC, the band gaps decrease by 0.15 eV, 0.33 eV and 0.86 eV for s/o-As, s/o-Sb and s/o-Bi, respectively. Accordingly, the direct fundamental band gap of s/o-Bi is predicted to be

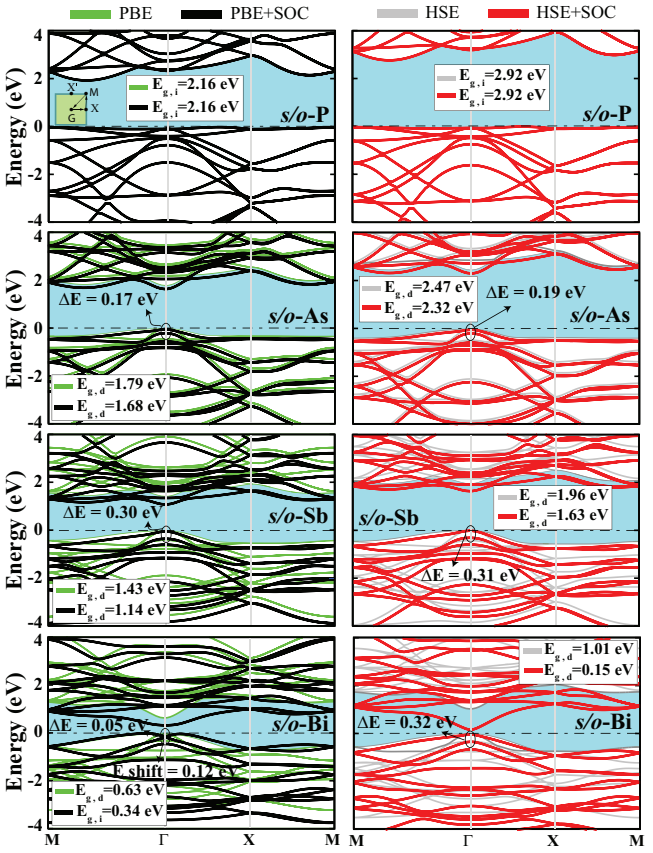

Figure 5. Energy band structures of s/o-X (X=P, As, Sb and Bi) structures calculated by PBE (green) , PBE+SOC (black), HSE (gray), HSE+SOC (red). Zero of energy is set to the top of the valence bands. The band gaps between conduction and valence bands are shaded and fundamental band gaps are indicated as direct $E_{g,d}$ or indirect $E_{g,i}$. ΔE is the spin-orbit splitting at the top of the valence band. E_{shift} is the energy difference of the state at the top of the valence band after Rashba splitting.

0.15 eV, which may attribute crucial properties relevant for topological insulator character.

The total and orbital projected densities of states of s/o-X structures are presented in Fig. 6. Sharp peak just at the edge of valence band of s/o-P is due to the flat bands of p_z-orbitals located at the top of valence band. Contribution of s-, p_x- and p_y-orbitals to the states at the edge of valence band is relatively smaller. However, the contribution of p_z-orbital to the states at the edge of the conduction band becomes comparable to those of p_x- and p_y-orbitals. The distributions of the state density near the edge of the valence bands of s/o-As, s/o-Sb and s/o-Bi differ from that of s/o-P due the energy lowering of the flat p_z-band along $M-\Gamma-X$ symmetry directions of BZ. Hence, contrary to s/o-P, the contribution of p_x- and p_y-orbitals to the states just at the top of the valence bands near the Γ-point exceed that of p_z-orbital for s/o-As and s/o-Sb. This is reversed for the edge of the conduction band, where the contribution of

Table III. Fundamental band gaps of s/o-X (X=P, As, Sb and Bi) calculated by PBE, PBE+SOC, HSE and HSE+SOC. Available PBE values calculated for b-X, w-X and aw-X are also given for the sake of comparison. Direct or indirect type of the band gap is indicated by (i) or (d).

		E_{gap} (eV)			
Method	structure	P	As	Sb	Bi
PBE	s/o	2.16(i)	1.79(d)	1.43(d)	0.63(d)
	b	1.91(i), 1.98[66]	1.57(i), 1.64[32]	1.07(i), 1.18[73]	0.49(d), 0.55[43]
	w	0.82(d), 0.90[66]	0.77(i), 0.83[32]	0.37(i), 0.54[73]	0.16(d), 0.16[43]
	aw	-	-	0.15(i), 0.16[36]	0.29(d), 0.31[43]
PBE+SOC	s/o	2.16(i)	1.68(d)	1.14(d)	0.34(i)
HSE	s/o	2.92(i)	2.47(d)	1.96(d)	1.01(d)
HSE+SOC	s/o	2.92(i)	2.32(d)	1.63(d)	0.15(d)

p_z-orbital is relatively higher. Moreover, this situation is unaltered with the inclusion of SOC to PBE calculations. Notably, for PBE bands the contributions of p_x-, p_y- and p_z-orbitals to the band edges of s/o-Bi is reminiscent of those s/o-As and s/o-Sb discussed above. However, once SOC is included to the PBE bands of s/o-Bi the order of p_z-orbital contribution to the band edges is inverted.

VI. DISCUSSIONS AND CONCLUSIONS

While 2D SL structures of group V elements in buckled honeycomb and washboard structures gain increasing research interest, here we predict another structure, which consists of buckled squares and octagon rings specified as s/o-X. This structure maintains group V elements threefold coordinated like buckled honeycomb and washboard structures and has even number of atoms in the primitive square lattice. Our analysis based on calculated mechanical properties, positive vibration frequencies and high-temperature, *ab-initio* molecular dynamic simulations indicates that suspended s/o-X structures are stable at room temperature and at least above it. Additionally, all of these structures are semiconductors with fundamental band gaps ranging from 3 eV to 0.15 eV. This renders s/o-structures of group V elements suitable for possible diverse applications in 2D electronics. In Fig. 7 we present the correlations of calculated values, the cohesive energy, formation energy, fundamental band gap, bond lengths, lattice constants and bucklings parameters of s/o-structures among group V elements. While structural parameters, such as lattice constants, bond lengths and buckling parameters increase with increasing row number of the group V elements, cohesive and formation energies, as well as fundamental band gap (PBE) decrease with increasing row number.

We found that the fundamental band gap of s/o-structure of any X element calculated by PBE is always largest among those of other stable SL phases, b-, w- and aw-structures of the same element. The effect of spin-orbit coupling on PBE bands is negligible for s/o-P, but becomes significant for s/o-Sb and s/o-Bi, where the band gap decreases by ∼0.3 eV. Upon HSE correction applied to PBE results, the band gap increases; the increment is as large as ∼0.8 eV for P and As, but is relatively smaller for Sb and Bi. The band gaps normally decrease also by the inclusion of the spin-orbit coupling to HSE correction. After the inclusion of the spin-orbit coupling to HSE correction, the band gap of s/o-Bi decreases from 1.01 eV to 0.15 eV, and the dominating orbital character of the states at the top of the valence band switches from p_x and p_y to p_z. Strong spin-orbit coupling can induce features indigenous to 2D topological insulator as in the asymmetric washboard structure of Bi.

The overall picture of the charge density plots of s/o-X is reminiscent of that of b-X. However, significant differences in the angles α_i, i=1-3 and β give rise to changes in the orbital combination of bonds. In this respect, the chemical activity of a s/o-X structures exhibits changes from b-X.

In conclusion, we predicted another type of single-layer phase of group V elements consisting of buckled square and octagon rings. They are dynamically and thermally stable even in their free standing form. We found that these s/o-structures of P, As, Sb and Bi are semiconductor.

ACKNOWLEDGMENTS

The computational resources are provided by TUBITAK ULAKBIM, High Performance and Grid Computing Center (TR-Grid e-Infrastructure). S.C. acknowledges financial support from the Academy of Sciences of Turkey (TUBA). This research was supported by Research Fund of the Adnan Menderes University under Project No.FEF-16016.

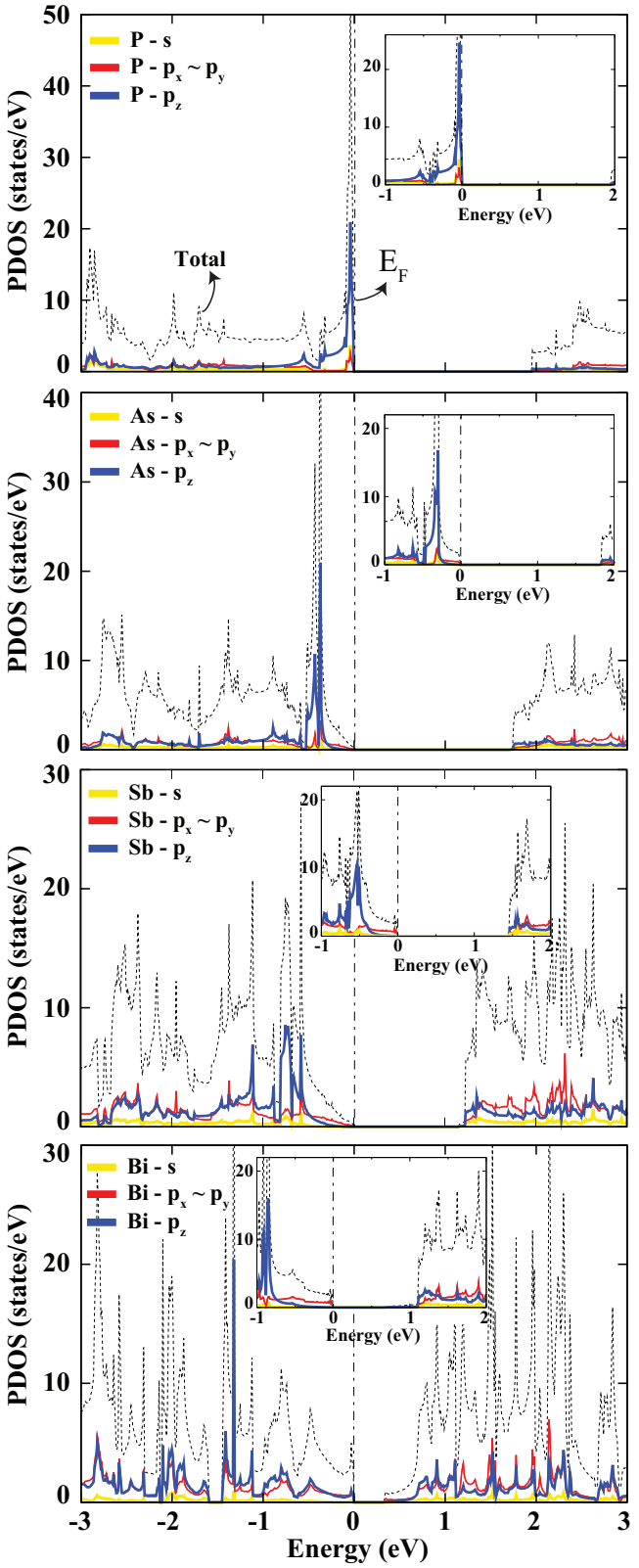

Figure 6. Total and orbital projected densities of states of s/o-X (X=P, As, Sb and Bi) structures calculated by PBE and PBE+SOC. Zero of energy is set to the top of the valence bands. The projected densities of states of s/o-X structures calculated by PBE are shown by inset near the edges of the fundamental band gap.

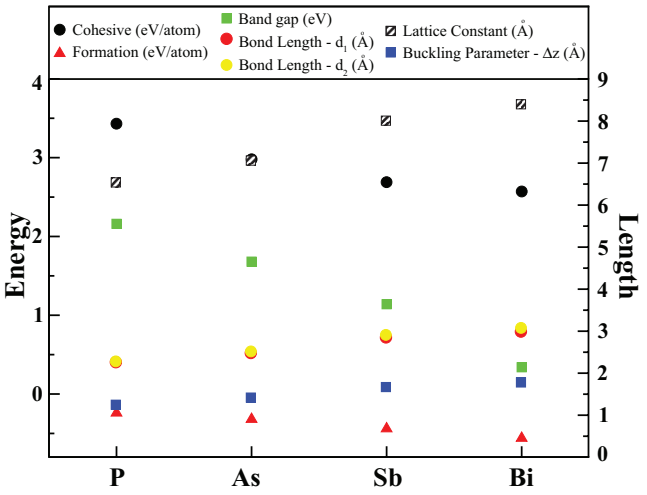

Figure 7. Correlations among the calculated values of cohesive energy, formation energy, band gap and bond lengths of different s/o-X structures treated in this study.

* ethem.akturk@adu.edu.tr
† ciraci@fen.bilkent.edu.tr

[1] K. S. Novoselov, A. K. Geim, S. V. Morozov, D. Jiang, Y. Zhang, S. V. Dubonos, I. V. Grigorieva and A. A. Firsov, Science, **306**, 666 (2004).
[2] K. S. Novoselov, A. K. Geim, S. V. Morozov, D. Jiang, M. I. Katsnelson, I. V. Grigorieva, S. V. Dubonos and A. A. Firsov, Nature **438**, 197 (2005).
[3] K. Novoselov, D. Jiang, F. Schedin, T. J. Booth, V. V. Khotkevich, S. V. Morozov and A. K. Geim, PNAS **102**, 10451 (2005).
[4] J.N. Coleman, M. Lotya, A. O'Neill, S. D. Bergin, P. J. King, U. Khan, K. Young, A. Gaucher, S. De, R. J. Smith, I. V. Shvets, S. K. Arora, G. Stanton, H. Y. Kim, K. Lee, G. T. Kim, G. S. Duesberg, T. Hallam, J. J. Boland, J. J. Wang, J. F. Donegan, J. C. Grunlan, G. Moriarty, A. Shmeliov, R. J. Nicholls, J. M. Perkins, E. M. Grieveson, K. Theuwissen, D. W. McComb, P. D. Nellist and V. Nicolosi, Science **331**, 568 (2011).
[5] C. Ataca, H. Şahin and S. Ciraci, J. Phys. Chem. C, **116**, 8983 (2012).
[6] E. Durgun, S. Tongay and S. Ciraci, Phys. Rev. B, **72**, 075420 (2005).
[7] S. Cahangirov, M. Topsakal, E. Aktürk, H. Şahin and S. Ciraci, Phys. Rev. Lett. **102**, 236804 (2009); S. Cahangirov, M. Topsakal and S. Ciraci, Phys. Rev. B **81**, 195120 (2010).
[8] P. Vogt, P. DePadova, C. Quaresima, J. Avila, E. Frantzeskakis, M. C. Asensio, A. Resta, B. Ealet and G. LeLay, Phys. Rev. Lett. **108**, 155501 (2012).
[9] M. E. Dávila and G. LeLay, Sci. Reports, **6**, 20714 (2016).
[10] H. Şahin, S. Cahangirov, M. Topsakal, E. Bekaroglu, E. Aktürk, R. T. Senger and S. Ciraci, Phys. Rev. B **80**, 155453 (2009).
[11] T. Y. Lu, X. X. Liao, H. Q. Wang and J.C Zheng, J. Mater.Chem. **22**, 10062 (2012).
[12] S. Lin, S. Zhang, X. Li, W. Xu, X. Pi, X. Liu, F. Wang, H. Wu and H. Chen, J. Phys. Chem. C, **119**, 19772 (2015).
[13] A. G. Gökçe and E. Aktürk, Appl. Surf. Sci. **332**, 147 (2015).
[14] C. J. Tong, H. Zhang, Y-N. Zhang, H. Liu and L. M. liu, J. Mater. Chem. A. **2**, 17971 (2014).
[15] P. Tsipas *et. al.*, Appl. Phys. Lett. **103**, 261605 (2013).
[16] Z. Al Balushi *et al.*, Nature Mater. (2016)
[17] R. H. Baughman and H. Eckhardt, J. Chem. Phys. **87**, 6687 (1987).
[18] A. Hirsch, Nature Mater. **9**, 868 (2010).
[19] F. Diederics, Nature **369**, 199 (1994).
[20] G. Li, Y. Li, H. Liu, Y. Guo, Y. Li and D. Zhu, Chem. Commun. **46**, 3256 (2010).
[21] V. O. Özçelik and S. Ciraci, J. Phys. Chem. C **117**, 2175 (2013).
[22] B. G. Kim and H. J. Choi, Phys. Rev. B **86**, 115435 (2012).
[23] V. N. Popov and P. Lambin, Phys. Rev. B , **88**, 075427 (2013).
[24] S. B. Ram, M. Aaditya and S. K. Abhishek, Sci. Reports **4**, 7164 (2014).
[25] S. Zhang, S. Liu, S. Huang, B. Cai, M. Xie, L. Qu, Y. Zou, Z. Hu, X. Yu and H. Zeng, Sci. China Mater. **58**, 929 (2015).
[26] W. Li, M. Guo, G. Zhang and Y. W. Zhang, Phys. Rev. B **89**, 205402 (2014).
[27] L. Li, Y. Yu, G. J. Ye, Q. Ge, X. Ou, H. Wu, D. Feng, X. H. Chen and Y. Zhang, Nat. Nanotechnol. **9**, 372 (2014).
[28] V. O. Özçelik, O. U. Aktürk, E. Durgun and S. Ciraci, Phys. Rev B **92**, 125420 (2015).
[29] Z. Zhu and D. Tománek, Phys. Rev. Lett. **112**, 176802 (2014).
[30] J. Guan, Z. Zhu and D. Tománek, ACS Nano, **8(12)**, 12763 (2014).
[31] M. Wu, H. Fu, L. Zhou, K. Yao and X.C. Zeng, NanoLett. **15**, 3557 (2015).
[32] C. Kamal and M. Ezawa, Phys. Rev. B **91**, 085423 (2015).
[33] Z. Zhang, J. Xie, D. Yang, Y. Wang, M. Si, and D Xue,

Appl. Phys. Express, **8**, 5 (2015).
[34] D. Kecik, E. Durgun and S. Ciraci, Phys. Rev. B (to be published); D. Kecik, E. Durgun and S. Ciraci, Phys. Rev. B (to be published).
[35] F. Ersan, E. Aktürk and S. Ciraci, J. Phys. Chem. C **120**, 14345 (2016).
[36] O. U. Aktürk, V. O. Özçelik and S. Ciraci, Phys. Rev. B**91**, 235446 (2015); O. Üzengi Aktürk, E. Aktürk and S. Ciraci, Phys. Rev. B **93**, 035450 (2016).
[37] S. Zhang, Z. Yan, Y. Li, Z. Chen and H. Zeng, Angew. Chem. Int. Ed. **54**, 3112 (2015).
[38] S. Zhang, Z. Yan, Y. Li, Z. Chen and H. Zeng, Angew. Chem. **127**, 3155 (2015).
[39] G. Wang, R. Pandey and S. P. Karna, ACS Appl. Mater.Interfaces, **7**, 11490 (2015).
[40] L. Cheng, H. Liu, X. Tan, J. Zhang, J. Wei, H. Lv, J. Shi and X. Tang, J. Phys. Chem. C, **118(2)**, 904 (2014).
[41] L. E. Díaz-Sánchez, A. H. Romero, M. Cardona, R. K. Kremer and X. Gonze, Phys. Rev. Lett. **99**, 165504 (2007).
[42] H. Iwasaki and T. Kikegawa, Acta Crystallogr. B. **53**, 353 (1997).
[43] E. Aktürk, O. U. Aktürk and S. Ciraci, Phys. Rev. B **94**, 014115 (2016).
[44] W. Yu, C. Y. Niu, Z. Zhu, X. Wang and W. B. Zhang, J. Mater. Chem. C. **4**, 6581 (2016).
[45] L. Kou, X. Tan, Y. Ma, H. Tahini, L. Zhou, Z. Sun, A. Du, C. Chen and S. C. Smith, 2D Materials, **2**, 045010 (2015).
[46] S. Grimme, J. Comput. Chem. **27**, 1787 (2006).
[47] P. E. Blöchl, Phys. Rev. B **50**, 17953 (1994).
[48] J. P. Perdew, K. Burke and M. Ernzerhof, Phys. Rev. Lett. **77**, 3865 (1996).
[49] G. Kresse and J. Furthmuller, Phys. Rev. B **54**, 11169 (1996).
[50] H. J. Monkhorst and J. D. Pack, Phys. Rev. B **13**, 5188 (1976).
[51] A. Togo and I. Tanaka, Scr. Mater. **108**, 1 (2015).
[52] J. Heyd, G. E. Scuseria and M. Ernzerhof, J. Chem. Phys. **118**, 18 (2003).
[53] J. Heyd, G. E. Scuseria and M. Ernzerhof, J. Chem. Phys. **118**, 8207,(2003); J. Chem. Phys. **124**, 21 (2006).
[54] J. Paier, M. Marsman, K. Hummer, G. Kresse, I. C. Gerber and J. G. Ángyán, J. Chem. Physics **124**, 154709 (2006).
[55] J. Paier, M. Marsman, K. Hummer, G. Kresse, I. C. Gerber and J. G. Ángyán,J. Chem. Phys. **125**, 249901 (2006).
[56] M. Topsakal, S. Cahangirov and S. Ciraci, Appl. Phys. Lett. **96**, 091912 (2011).
[57] M. Sun, S. Wang, J. Yu and W. Tang, Appl. Surf. Sci. **392**, 46 (2017).
[58] V. Vierimaa, A. V. Krasheninnikov and H. P. Komsa, Nanoscale, **8**, 7949 (2016).
[59] Q. Wei and X, Peng, Appl. Phys. Lett., **104**, 251915 (2014).
[60] J. W. Jiang and H. S. Park, J. Phys. D: Appl. Phys., **47**, 385304 (2014).
[61] J. Lee, W. C. Tian, W. L. Wang and D. X. Yao, Sci. Reports, **5**, 11512 (2015).
[62] B. Noläng, 0. Eriksson and B. Johansson, J. Phys. Chem. Solids, **51**, 9 (1990).
[63] J.R. Feng and G. C. Wang, RSC Adv., **6**, 22277 (2016).
[64] H. Kim, J. Korean Phys. Soc., **64(4)**, 547 (2014).
[65] Y. Aierken, D. Çakır, C. Sevik and F.M. Peeters, Phys. Rev. B **92**, 081408 (2015).
[66] J. Guan, Z. Zhu and D. Tománek, Phys. Rev. Lett. **113**, 046804 (2014).
[67] H. Guo, N. Lu, J. Dai, X. Wu and X. C. Zeng, J. Phys. Chem. C, **118(25)**, 14051 (2014).
[68] S. Mardanya, V. K. Thakur, S. Bhowmick and A. Agarwal, Phys. Rev. B, **94**, 035423 (2016).
[69] M. Y. Liu, Y. Huang, Q. Y. Chen, C. Cao and Y. He, Sci. Reports, **6**, 29114 (2016).
[70] L. Kou, Y. Ma, X. Tan, T. Frauenheim, A. Du and S. Smith, J. Phys. Chem. C, **119**, 6918 (2015).
[71] C. Kittel, Introduction to Solid State Physics, 8th ed. (John Wiley & Sons, New York, 1996).
[72] C. S. Barrett, P. Cucka and K. Haefner, Acta Cryst. **16**, 451 (1963).
[73] D. Singh, S. K. Gupta, Y. Sonvane and I. Lukačević, J. Mater. Chem. C, **4**, 6386 (2016).